

**From Precipitation to Prediction: Using ConvLSTM
Models for Comprehensive River Runoff Forecasting**

Florian Börgel¹, Sven Karsten¹, Karoline Rummel¹

¹Leibniz-Institute for Baltic Sea Research Warnemünde,

5 **Abstract**
 6 a

7 **Plain Language Summary**
 8 b

9 **1 Introduction**

10 River runoff is an important component of the global water cycle as it comprises
 11 about one third of the precipitation over land areas (Hagemann et al., 2020). Therefore,
 12 accurate runoff forecasting is crucial for effective water resources management,
 13 particularly over extended periods (Fang et al., 2019; Tan et al., 2018). In the context
 14 of climate change studies, river runoff is usually generated in two ways. First,
 15 river runoff as input for ocean models can be created using hydrological models such
 16 as the Hydrological Discharge (HD) model (Hagemann et al., 2020). HD models
 17 calculate the water balance using hydrological processes (e.g. snow, glaciers, soil
 18 moisture, groundwater contribution). It represents a complex forecasting tool that
 19 uses underlying physical processes. The second approach uses data-driven models
 20 that integrate statistical correction, using land surface schemes of global or regional
 21 climate models [missing].

22 With the recent rise of machine learning in climate research various model archi-
 23 tectures have also been tested for river runoff forecasting. Common approaches
 24 employ feed-forward artificial neural networks, support vector machines, adaptive
 25 neuro-fuzzy inference systems, and notably, Long Short-Term Memory (LSTM) neu-
 26 ral networks that have gained traction for long-term hydrological forecasting due
 27 to their excellent performance (**humphrey2016hybrid?**; **huang2014monthly?**;
 28 **ashrafi2017fully?**; **liu2020streamflow?**; **fang2022application?**; **kratzert2018rainfall?**).

29 LSTM networks, first introduced by (**hochreiter1997long?**) , are an evolution of
 30 the classical Recurrent Neural Networks (RNNs). A significant advantage of this ar-
 31 chitecture is the memory cell's ability to retain gradients. This mechanism addresses
 32 the vanishing gradient problem, where, as input sequences elongate, the influence of
 33 initial stages becomes harder to capture, causing gradients of early input points to
 34 approach zero. LSTMs have shown stability and efficacy in sequence-to-sequence pre-
 35 dictions. This performance in modeling long-range dependencies has been validated
 36 in various studies [missing].

37 However, a limitation of LSTMs is their inability to effectively capture two-dimensional
 38 structures, an area where Convolutional Neural Networks (CNNs) excel. Recogniz-
 39 ing this limitation, SHI et al. (2015) proposed a Convolutional LSTM (ConvLSTM)
 40 architecture, which combines the strengths of both LSTM and CNN. The ConvL-
 41 STM network has been proven useful for spatio-temporal applications such as precip-
 42 itation nowcasting (SHI et al., 2015), flood forecasting (**moishin2021designing?**),
 43 and river runoff forecasting (**ha2021?**; **zhu2023spatiotemporal?**).

44 In this work, we demonstrate that ConvLSTM networks are a reliable method for
 45 predicting multiple rivers simultaneously, using only atmospheric forcing, even in the
 46 absence of a fully functional hydrological model with a complex parameterization.
 47 Still, data of a suitable HD model is used as reference to train the network. We
 48 use the Baltic Sea catchment as an example to illustrate our approach. Although
 49 the methodology we propose is universally applicable across various geographic re-
 50 gions, the Baltic Sea represents a challenging region due to its unique hydrological
 51 characteristics, being nearly decoupled from the open ocean (see Figure). As a con-
 52 sequence, the salinity of the Baltic Sea is driven to a large part by freshwater supply
 53 from rivers. Freshwater enters the Baltic Sea through river runoff or positive net
 54 precipitation (precipitation minus evaporation) over the sea surface. The net precip-

55 itation accounts for 11 % and the river input for 89 % of the total freshwater input
 56 (**meier2002simulated?**). Modelling the Baltic Sea is therefore to a large part the
 57 result of the quality of the river input, that is used for the simulation. This makes
 58 the accurate modeling of river runoff especially critical for simulations pertaining to
 59 the Baltic Sea.

60 The main focus of this work is to present a ConvLSTM architecture that is able to
 61 predict daily river runoff for 97 rivers across the Baltic Sea catchment (Section 2).
 62 To train the network, we use data from the E-HYPE HD model [missing] as refer-
 63 ence output data and data from the UERRA project (Uncertainties in Ensembles of
 64 Regional Re-Analyses, <http://www.uerra.eu/>), as atmospheric forcing (Section 3).
 65 The quality of the model is evaluated in ?@sec-sec-evaluation and subsequently
 66 the trained ConvLSTM is used in combination with the MOM5 ocean model for the
 67 Baltic Sea (Neumann et al., 2021) (Section 4.2). The obtained results are further
 68 discussed in Section 5 and concluded in Section 6.

69 **2 Implemented model architecture**

70 **2.1 The main idea**

71 We assume that the runoff at a specific point in time t for all N_r considered rivers,
 72 collected in the vector $\vec{R}^t \in \mathbb{R}^{N_r}$, can be accurately approximated by a functional
 73 $\vec{M}(\{X_k^t[x, y, \tau]\})$ of $k = 1, \dots, N_k$ atmospheric fields $X_k^t[x, y, \tau]$ which are known for
 74 the past $\tau = 1, \dots, N_\tau$ time instances. This relationship is expressed as:

$$\vec{R}^t = \vec{M}(\{X_k^t[x, y, \tau]\}).$$

75 The atmospheric fields are evaluated over a spatial domain $x = 1, \dots, N_x$ and
 76 $y = 1, \dots, N_y$ which is sufficiently large to capture all significant local and non-local
 77 contributions of the atmospheric fields to the river runoff.

78 Typically, such a mapping is realized using a hydrological model that simulates all
 79 relevant physical processes, transforming variables like precipitation and evapora-
 80 tion into river runoff. This process relies heavily on domain knowledge to tune all
 81 parameters to reasonable values.

82 As an alternative, we propose that this functional can be adequately represented by
 83 a combination of a convolutional Long-Short Term Memory (ConvLSTM) model
 84 with a subsequent fully connected (FC) neural network. This approach eliminates
 85 the need for detailed knowledge of the involved processes and their modeling. In-
 86 stead, these features can be “learned” by the network in an automated manner,
 87 i.e. all free parameters are optimized such that the network’s output reproduces best
 88 the HD model data with given atmospheric input fields. Our proposed network ar-
 89 chitecture is visualized in Figure 1 and described in detail in the following sections.
 90 To provide an overview, we will discuss the main components of this architecture
 91 one-by-one.

92 **2.2 The ConvLSTM network**

93 **2.2.1 The LSTM approach**

94 Before turning directly to the ConvLSTM the simpler architecture of the plain Long-
 95 Short Term Memory (LSTM) model is examined which serves as a foundation for
 96 understanding the more complex ConvLSTM.

97 The LSTM, a specialized form of Recurrent Neural Networks (RNNs), is specifically
 98 designed to model temporal sequences $\vec{X}^t[1], \dots, \vec{X}^t[\tau], \dots, \vec{X}^t[N_\tau]$ of N_τ input quanti-
 99 ties $\vec{X}^t[\tau] = (X_k^t[\tau]) \in \mathbb{R}^{N_k}$. This sequence is taken from a dataset given in form of
 100 a time series $\{\vec{X}^t\}$ with the endpoint coinciding with the specific element in the time
 101 series connected to time t , i.e. $\vec{X}^t[N_\tau] \equiv \vec{X}^t$, see Figure 1. Here, N_k represents the
 102 number of input “channels,” which can correspond to different measurable quanti-

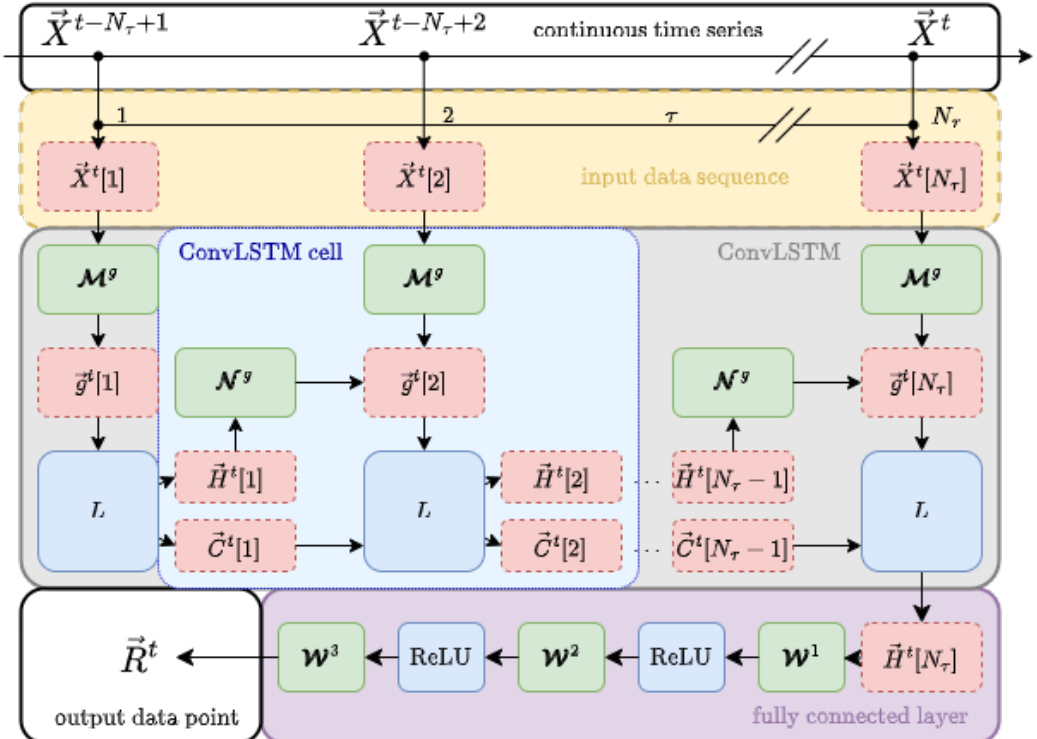


Figure 1: **Combined ConvLSTM and FC network architecture.** The starting point is the continuous time series of input data $\{\vec{X}^t\}$, upper white block. From this series, a contiguous sequence of N_τ elements (yellow block) is used to feed a chain of N_τ connected ConvLSTM cells (light blue block) building the ConvLSTM network (grey block). The input sequence is mapped via weighting matrices \mathcal{M}^g (green blocks) onto gate vectors $\vec{g}^t[\tau]$. The gate vectors are then used to update the cell state $\vec{C}^t[\tau - 1]$ and the hidden state $\vec{H}^t[\tau - 1]$ of the last ConvLSTM cell to the current values $\vec{C}^t[\tau]$ and $\vec{H}^t[\tau]$, respectively. The update is performed with the LSTM core equations collectively described by the mapping L , see Equation 2. The weighting matrices \mathcal{N}^g (green blocks) control how much of the last hidden state enters the updated state. The final output of the ConvLSTM $\vec{H}^t[\tau]$ is then propagated to a FC network, which itself is a chain of three FC layers consisting of weighting matrices \mathcal{W} and connected via ReLU functions, see Section 2.3. The final result is the river runoff \vec{R}^t for all rivers considered at the current time instance t (white block on the lower left). Note that all bias vectors are omitted for the sake of clarity. See text for more information.

ties. The LSTM's unique design allows it to adeptly handle long-range dependencies, setting it apart from traditional RNNs in terms of accuracy (see Figure 2).

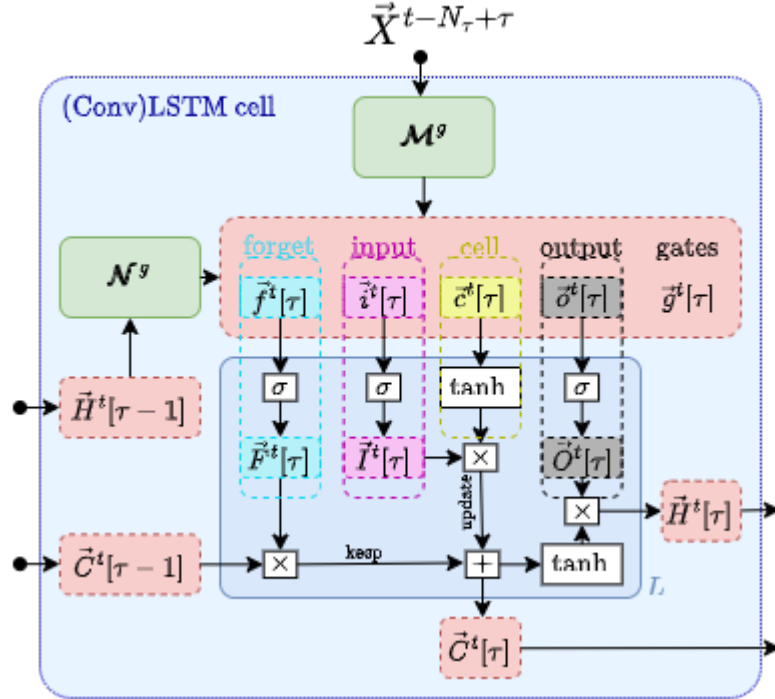


Figure 2: **Inner structure of a Long Short-Term Memory Cell.** See Figure 1 and text for information.

The key component of the LSTM's innovation is its cell state, $\vec{C}^t[\tau] = (C_h^t[\tau]) \in \mathbb{R}^{N_h}$, which stores state information, also referred to as *long-term memory*. This state information complements the so-called hidden state vector $\vec{H}^t[\tau] = (H_h^t[\tau]) \in \mathbb{R}^{N_h}$, which is also known from simpler neural network architectures. In case of the LSTM, the hidden state vector plays the role of the *short-term memory*. The cell state and the hidden state are vectors, where each element is associated with one of the N_h hidden layers, labeled by h , which are internal, *artificial* degrees of freedom that enable the high adaptability of neural networks. These two state vectors are determined through several self-parameterized gates, all in the same vector space as $\vec{C}^t[\tau]$, see Figure 2 for a visualization.

In particular, the forget gate $\vec{F}^t[\tau]$ defines the portion of the previous (long-term memory) cell state $\vec{C}^t[\tau - 1]$ that should be kept, see dashed cyan box therein. The input gate $\vec{I}^t[\tau]$ controls the contribution of the current input used to update the long-term memory, $\vec{C}^t[\tau]$ (magenta and yellow boxes). The output gate, $\vec{O}^t[\tau]$, then determines how much of this updated long-term memory contributes to the new (short-term memory) hidden state, $\vec{H}^t[\tau]$ (black dashed box).

For a fixed point τ in the sequence, the action of a LSTM cell, i.e. the connection between the input $\vec{X}^t[\tau]$, the various gates and the state vectors, is mathematically given as follows.

First, the elements of the input sequence together with the hidden state are mapped onto auxiliary gate vectors, collectively denoted by $\vec{g}^t[\tau] = (g_h^t[\tau]) \in \mathbb{R}^{N_h}$, via

$$g_h^t[\tau] = \mathcal{M}_{hk}^g X_k^t[\tau] + \mathcal{N}_{hh'}^g H_{h'}^t[\tau - 1] + \mathcal{B}_h^g ,$$

where $g = i, f, o, c$ stands for the input, forget, output and cell-state gate, respectively and Einstein's summation convention is employed, i.e. indices that appear twice are summed over. The calligraphic symbols \mathcal{M}_{hk}^g , $\mathcal{N}_{hh'}^g$, and \mathcal{B}_h^g are the free parameters of the network that are optimized for the given problem during the training, which is at the heart of the any machine learning approach. The matrix $\mathcal{M}^g = (\mathcal{M}_{hk}^g) \in \mathbb{R}^{N_h \times N_k}$ can be interpreted as a Markovian-like contribution of the current input $\vec{X}^t[\tau]$ to the gates, whereas the $\mathcal{N}^g = (\mathcal{N}_{hh'}^g) \in \mathbb{R}^{N_h \times N_h}$ scales a non-Markovian part determined by the hidden state of the last sequence point $\tau - 1$. The vector $\vec{\mathcal{B}}^g = (\mathcal{B}_h^g) \in \mathbb{R}^{N_h}$ is a learnable bias. It should be stressed that these parameters do neither depend on t nor on τ and are thus optimized once for the complete dataset $\{\vec{X}^t\}$.

Note that this mapping is sometimes extended by a contribution to the $g_h^t[\tau]$ from the past cell state $\vec{C}^t[\tau - 1]$ [missing]. Nevertheless, this mechanism called “peeping” is not further considered in this work.

For the sake of brevity, we can write the mapping more compactly in matrix-vector form as

$$\vec{g}^t[\tau] = \mathcal{M}^g \vec{X}^t[\tau] + \mathcal{N}^g \vec{H}^t[\tau - 1] + \vec{\mathcal{B}}^g \quad (1)$$

Second, the actual gate vectors are computed by the core equations of the LSTM as proposed by (**hochreiter1997long?**):

$$\begin{aligned} \vec{I}^t[\tau] &= \sigma(\vec{i}^t[\tau]) \\ \vec{F}^t[\tau] &= \sigma(\vec{f}^t[\tau]) \\ \vec{O}^t[\tau] &= \sigma(\vec{o}^t[\tau]) \\ \vec{C}^t[\tau] &= \vec{F}^t[\tau] \circ \vec{C}^t[\tau - 1] + \vec{I}^t[\tau] \circ \tanh(\vec{c}^t[\tau]) \\ \vec{H}^t[\tau] &= \vec{O}^t[\tau] \circ \tanh(\vec{C}^t[\tau]) , \end{aligned} \quad (2)$$

where σ denotes the logistic sigmoid function, \tanh is the hyperbolic tangent and the \circ stands for the Hadamard product (all applied in an element-wise fashion to the vectors). In the last two equations the role of the input, forget and output gates as described above becomes apparent.

The third step in a single layer LSTM (as employed for the work presented here) is then to provide the output of the current LSTM cell, i.e. $\vec{H}^t[\tau]$ and $\vec{C}^t[\tau]$, to the subsequent LSTM cell that processes the next element $\vec{X}^t[\tau + 1]$ of the input sequence.

The full action of the LSTM network up to the end of the sequence can be written as a nested function call

$$(\vec{H}^t[N_\tau], \vec{C}^t[N_\tau]) = L(\vec{X}^t[N_\tau], L(\vec{X}^t[N_\tau - 1], \dots L(\vec{X}^t[1], (\vec{H}^t[0], \vec{C}^t[0])) \dots)) , \quad (3)$$

where $L(\vec{X}^t[\tau], (\vec{H}^t[\tau - 1], \vec{C}^t[\tau - 1]))$ represents Equation 1 and Equation 2. For the present work, the initial conditions are chosen as $\vec{H}^t[0] = \vec{C}^t[0] = 0$, which simply means that there is no memory longer than N_τ time steps.

The final output of the ConvLSTM chain, $\vec{H}^t[N_\tau]$ and $\vec{C}^t[N_\tau]$, encode information on the full input sequence ending at time t . This information has to be decoded via an appropriate subsequent network, as it is described in the Section 2.3.

2.2.2 Combining the LSTM with spatial convolution

Although the plain LSTM has high performance in handling temporal sequences of point-like quantities it is not designed to recognize spatial features in sequences of two-dimensional maps as atmosphere-ocean interface fields. To address this limitation we employ a ConvLSTM architecture as described in the following.

In this kind of network the elements of the input sequence are given as spatially varying fields $\vec{X}^t[\tau] = (X_k^t[x, y, \tau]) \in \mathbb{R}^{N_k \times (N_x \times N_y)}$, where $x \in [1, N_x]$ and $y \in [1, N_y]$ run over the horizontal and vertical dimensions of the map, respectively. In order to enable the “learning” of spatial patterns, the free parameters of the network are replaced by two-dimensional convolution kernels $\mathcal{M}^g = (\mathcal{M}_{hk}^g[\xi, \eta]) \in \mathbb{R}^{(N_h \times N_k) \times (N_\xi \times N_\eta)}$ and $\mathcal{N}^g = (\mathcal{N}_{hh'}^g[\xi, \eta]) \in \mathbb{R}^{(N_h \times N_h) \times (N_\xi \times N_\eta)}$. The width and the height of the kernels are given by N_ξ and N_η , respectively and $\xi \in [-(N_\xi - 1)/2, (N_\xi - 1)/2]$, $\eta \in [-(N_\eta - 1)/2, (N_\eta - 1)/2]$, where, without loss of generality, we assume odd numbers for the kernel sizes.

The mapping from the input quantities to the gates is then given by a convolution with these kernels

$$g_h^t[x, y, \tau] = \mathcal{M}_{hk}^g[\xi, \eta] X_k^t[x - \xi, y - \eta, \tau] + \mathcal{N}_{hh'}^g[\xi, \eta] H_{h'}^t[x - \xi, y - \eta, \tau - 1] + \mathcal{B}_h^g .$$

again with Einstein’s convention imposed.

It becomes immediately apparent that in case of the ConvLSTM, the gate and state vectors must become vector fields ($\in \mathbb{R}^{N_h \times (N_x \times N_y)}$) as well. We can write this mapping in the same way as Equation 1 but with replacing the normal matrix-vector multiplication by a convolution (denoted with $*$), i.e.

$$\vec{g}^t[\tau] = \mathcal{M}^g * \vec{X}^t[\tau] + \mathcal{N}^g * \vec{H}^t[\tau - 1] + \vec{\mathcal{B}}^g$$

The subsequent processing of the $\vec{g}^t[\tau]$ remains symbolically the same as presented in Equation 2 but with all appearing quantities now meaning vector fields instead of simple vectors.

In summary, the ConvLSTM is designed for processing tasks that demand a combined understanding of spatial patterns and temporal sequences in data. It merges the image-processing capabilities of Convolutional Neural Networks (CNNs) with the time-series modeling of Long Short-Term Memory (LSTM) networks.

2.3 Fully connected layer

As stated in Section 2.2.1, the final output $\vec{H}^t[N_\tau]$ and $\vec{C}^t[N_\tau]$ of the ConvLSTM encode information on the full input sequence. In order to contract this information to obtain the runoff vector \vec{R}^t representing the N_r rivers, we propose to subject the final short-term memory (i.e. the hidden state $\vec{H}^t[N_\tau]$) to an additional FC network.

In particular, the dimensionality of the vector field $\vec{H}^t[N_\tau]$ is sequentially reduced by three nested FC layers, each connected to the other by the Rectified Linear Unit (ReLU), see Figure 1. Integrating out artificial degrees of freedom in a step-wise fashion has turned out to be beneficial [missing].

Spelled out in mathematics, the runoff of the r -th river is then obtained via (using Einstein’s convention)

$$R_r^t = \mathcal{W}_{rb}^3 \text{ReLU}(\mathcal{W}_{ba}^2 \text{ReLU}(\mathcal{W}_{ah}^1[x, y] H_h^t[x, y, N_\tau] + \mathcal{B}_a^1) + \mathcal{B}_b^2) + \mathcal{B}_r^3 ,$$

where $a = 1, \dots, N_a$, $b = 1, \dots, N_b$ and the hyper parameters N_a and N_b are chosen such that $N_h \cdot N_x \cdot N_y > N_a > N_b > N_r$ in order to achieve the aforementioned step-by-step reduction of dimensionality. The weights \mathcal{W} and biases \mathcal{B} stand for parameters that are optimized during the training of the network.

In matrix-vector notation this can be compressed to

$$\vec{R}^t = \mathcal{W}^3 \text{ReLU} \left(\mathcal{W}^2 \text{ReLU} \left(\mathcal{W}^1 \vec{H}^t[N_\tau] + \vec{\mathcal{B}}^1 \right) + \vec{\mathcal{B}}^2 \right) + \vec{\mathcal{B}}^3. \quad (4)$$

Combining Equation 4 with Equation 3 provides finally an explicit formula for the initial assumption of modelling the runoff for time t as a functional of a sequence of atmospheric fields, i.e.

$$\begin{aligned} \vec{R}^t &= \vec{M}(\{X_k^t[x, y, \tau]\}) \\ &= \mathcal{W}^3 \text{ReLU} \left(\mathcal{W}^2 \text{ReLU} \left(\mathcal{W}^1 \vec{L}_H \left(\vec{X}^t[N_\tau], L \left(\vec{X}^t[N_\tau - 1], \dots L \left(\vec{X}^t[1], (0, 0) \right) \dots \right) \right) + \vec{\mathcal{B}}^1 \right) + \vec{\mathcal{B}}^2 \right) + \vec{\mathcal{B}}^3, \end{aligned}$$

where the \vec{L}_H means that only the hidden state vector of the final ConvLSTM call is forwarded to the FC layer.

In Section 3, we present the employed model and data setup as well as the choice for all mentioned hyper parameters that lead to an adequate model performance after training.

3 Technical details

3.1 Runoff data used for training

The runoff data covering the period 1979 to 2011 is based on an E-HYPE hindcast simulation that was forced by a regional downscaling of ERA-Interim ([dee2011?](#)) with RCA3 ([theross?](#)) and implemented into NEMO-Nordic ([hordoir2019?](#)) as a mass flux. For the periods before (1961 to 1978) and after (2012 to 2018) additional spatial temporal corrections have been applied to the runoff data, and have therefore been ignored. The quality of the runoff was extensively evaluated. For more information see ([gröger2022?](#)) and references therein.

3.2 Atmospheric Forcing

The UERRA-HARMONIE regional reanalysis dataset was developed as part of the FP7 UERRA project (Uncertainties in Ensembles of Regional Re-Analyses, <http://www.uerra.eu/>). The UERRA-HARMONIE system represents a comprehensive, high-resolution reanalysis covering a wide range of essential climate variables. This dataset encompasses data on air temperature, pressure, humidity, wind speed and direction, cloud cover, precipitation, albedo, surface heat fluxes, and radiation fluxes from January 1961 to July 2019. With a horizontal resolution of 11 km and analyses conducted at 00 UTC, 06 UTC, 12 UTC, and 18 UTC, it also provides hourly resolution forecast model data. UERRA-HARMONIE is accessible through the Copernicus Climate Data Store (CDS, <https://cds.climate.copernicus.eu/#!/home>), initially produced during the UERRA project and later transitioned to the Copernicus Climate Change Service (C3S, <https://climate.copernicus.eu/copernicus-regionalreanalysis-europe>).

3.3 Ocean Model

To simulate the Baltic Sea, we use a coupled 3-dimensional ocean model Baltic Sea, called the Modular Ocean Model (MOM). This model uses a finite-difference method to solve the full set of primitive equations to calculate the motion of water and the transport of heat and salt. The K-profile parameterization (KPP) was used as turbulence closure scheme. The model's western boundary opens into the Skagerrak and connects the Baltic Sea to the North Sea. The maximum depth was set at 264 meters. A more detailed description of the setup can be found in ([gröger2022?](#)).

3.4 Neural network hyper parameters

During training, the following set of hyper parameters has turned out to yield sufficient quality of the results for the present study:

Table 1: Hyperparameters

Parameter name	Parameter size
Channel size	4
Num. hidden layer	9
Num. timesteps	30
Conv. kernel size	(7,7)
Num. ConvLSTM layers	1
Batch size	50
Learning Rate	1e-3 with CosineAnnealing

As input the model receives $N_\tau = 30$ days of atmospheric surface fields temperature, precipitation, specific humidity and wind speed, with a daily resolution to predict the river runoff \vec{R} (Figure 3).

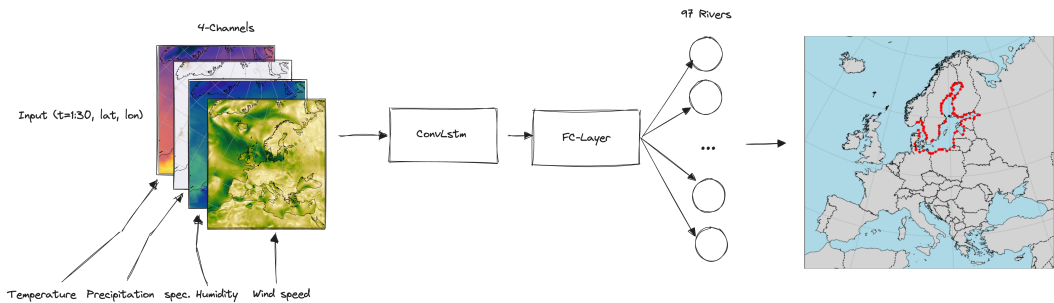


Figure 3: Schematic structure of the ConvLSTM implementation for river runoff forecasting.

The choice of atmospheric fields was based on the assumption that the runoff should be mainly given by the net precipitation (precipitation minus evaporation). The evaporation flux is often calculated as a function of wind speed, the air's humidity, the air's density and the involved turbulent exchange coefficients (Karsten et al., 2024), where the latter two are influenced by the air temperature.

4 Results

4.1 ConvLSTM model evaluation

The model was trained with daily data for the period 1979 to 2011, as this period represents the only period of E-HYPE without further bias correction applied to the runoff to match observations. The data was divided into randomly chosen splits of 80% training data, 10% validation data to evaluate the performance of the model during training, and 10% test data which is finally used to evaluate the performance of the model after training. The model was trained for 400 epochs and the model weights with the lowest mean squared error during training have been stored.

The accuracy of the model is displayed in Figure 4. As mentioned above, for this evaluation, the model's output is compared to the test data, which, importantly, the model has not seen yet during the training. Which river is shown here? The left panel a) illustrates the relative prediction error in relation to the original E-HYPE data, indicating that, on daily timescales, the model can predict river runoff with an accuracy of $\pm 5\%$. The overall correlation is 0.997 with the resulting error metrics yielding a root mean square error (RMSE) of $323.99 \text{ m}^3/\text{s}$ and mean absolute error

(MAE) of $249.51 \text{ m}^3/\text{s}$. While the model's performance is satisfactory, the discrepancies between the actual values and the predictions could partly be attributed to the use of a different atmospheric dataset than the one originally used to drive the E-HYPE model. However, by applying a rolling mean with a 5-day window, the prediction error is reduced to less than 1%, which is acceptable for the purposes of climate modeling. Lastly, the right panel demonstrates that the distribution of residuals follows a Gaussian shape, suggesting that our model does not exhibit bias by systematically over or underestimating river runoff values.

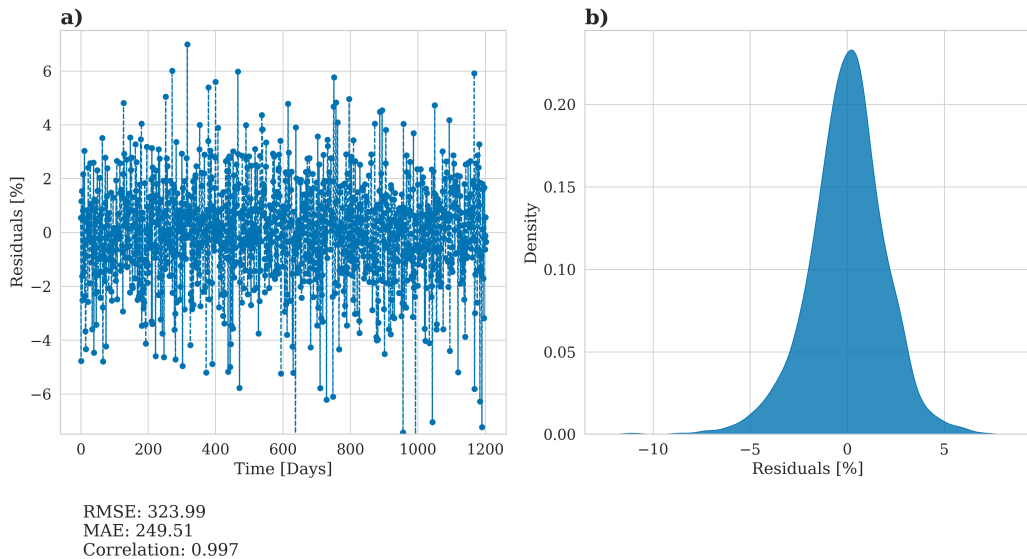


Figure 4

The time axis should be improved here and in all other time series plots.

In the following the model's performance to reproduce the total river runoff as well as the inflow of the four largest rivers into the Baltic Sea is addressed. Figure 5 shows the predicted and the original river runoff in comparison to the test dataset. The predicted total river runoff for the Baltic Sea is closely matching the original data, see panel a) therin. Zooming in on the largest individual rivers (panels b-e), it can be seen that also the prediction of the individual rivers is close to the original data.

4.2 Application of the ConvLSTM in combination with an ocean model
 Lastly, we evaluate the performance of the ConvLSTM by incorporating the predicted river runoff as hydrological forcing into the ocean model MOM5. This provides a robust validation of the runoff model against more complex real world conditions and is thereby ensuring that the predictions accurately reflect the impact of the river discharge on the ocean dynamics. This in turn validates that the temporal and spatial variability of river runoff is well captured by ConvLSTM and that the residuals shown in Figure 4 are indeed insignificant when it comes to realistic applications.

Figure 6 shows the salinity comparison between the original E-HYPE river runoff and the predicted river runoff at BY15 - a central station in the Baltic Sea, east of

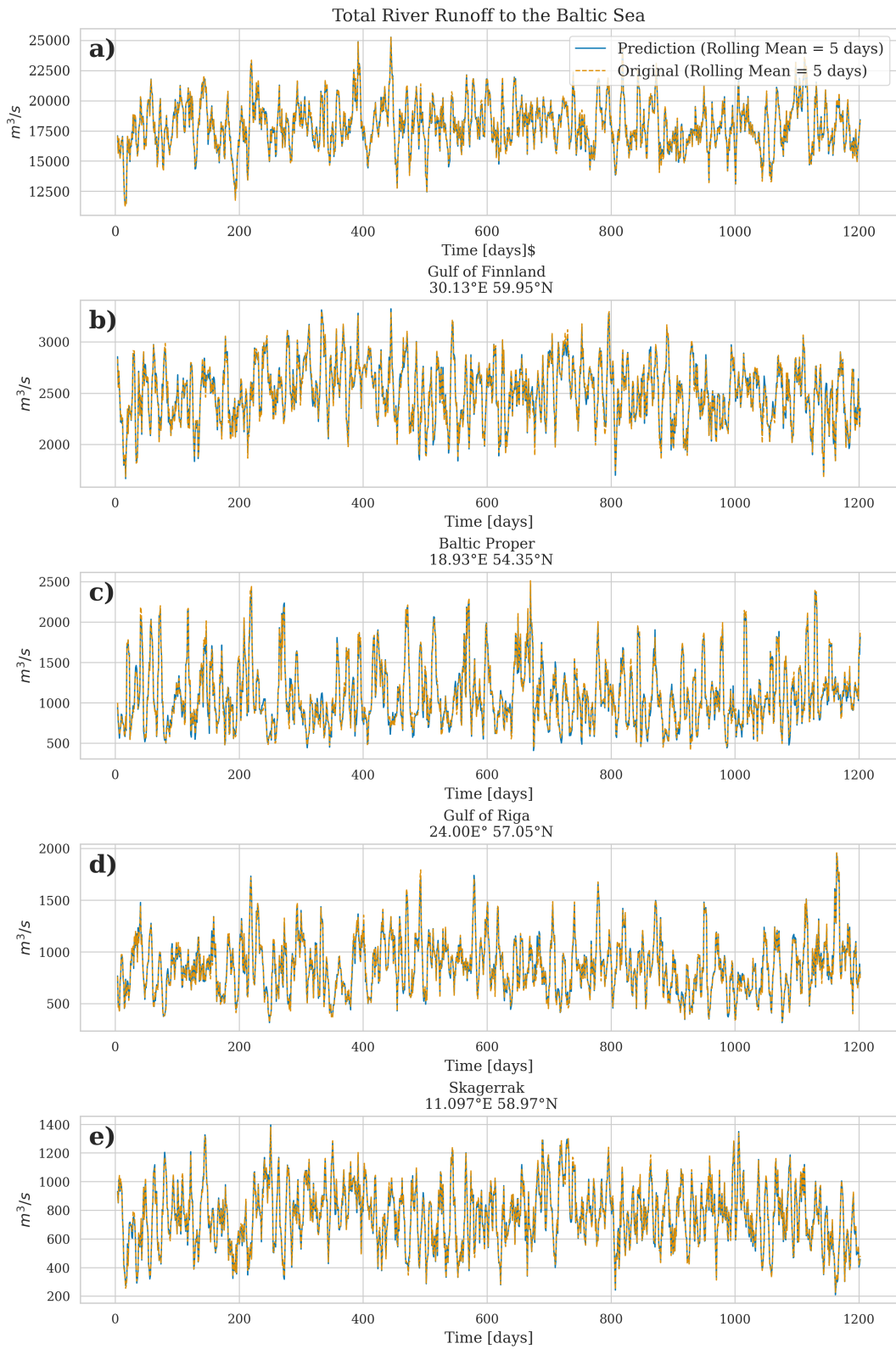


Figure 5

291 the Gotland island. It can be seen that the model simulation using the predicted
 292 river runoff by the ConvLSTM is closely mirroring the control simulation, that is
 293 forced with the E-HYPE runoff. The upper panel a) shows the surface salinity, rep-
 294 resenting the high-frequency variations in the salinity, which is heavily affected by
 295 river runoff. The lower panel b) shows the bottom salinity which in turn is low-
 296 frequency feature in the Baltic Sea that is also well reproduced with the ConvLSTM
 297 predictions.

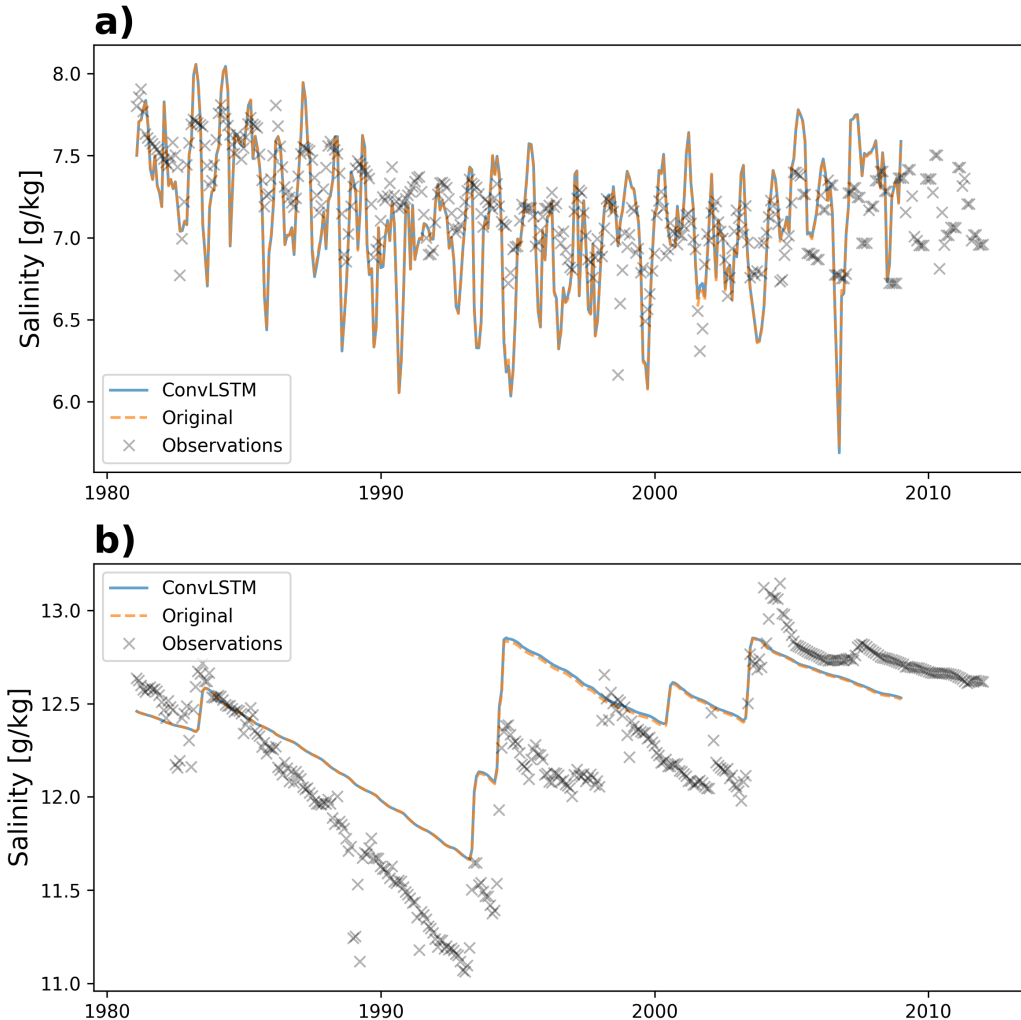


Figure 6

298 The final evaluation of the ConvLSTM model concentrates on the spatial accuracy
 299 of river runoff predictions as visualized in Figure 7. Panel a) therein exhibits the
 300 vertically averaged salinity for the period 1981 to 2011 in the reference simulation.
 301 It highlights the strong horizontal gradients and complex topographic features in
 302 the Baltic Sea, as evidenced by salinity variations in deeper waters, captured by the
 303 vertical integration. In panel b), these reference results are compared to the ConvL-
 304 STM simulation by showing the percentage difference in vertically averaged salinity.
 305 Overall, the differences remain below 1%, except in the Gulf of Riga (22–24°E, 56.5–

306 58.5°N for orientation), where the runoff is dominated by the Daugava river. Here
 307 the difference is approximately 1%.

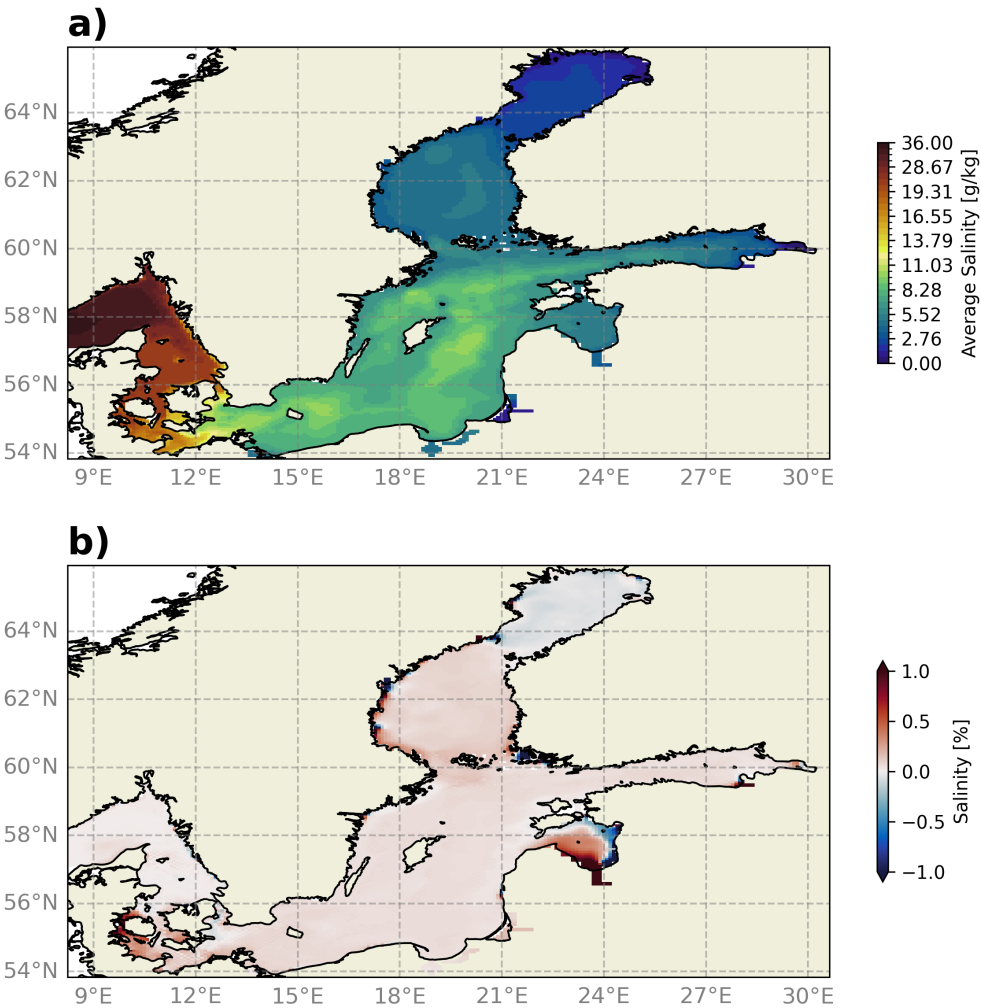


Figure 7

308 5 Discussion

309 With the increasing demand of decision makers for regional climate projections, that
 310 allow to quantify regional climate change impacts, the availability of precise hydro-
 311 logical forecasting becomes invaluable. The quality of a projection for a coastal sea
 312 such as the Baltic Sea is too large parts based on the quality of the hydrological con-
 313 ditions. In this work we analyze the implementation of a ConvLSTM networks for
 314 predicting river runoff, highlighting its potential to enhance river runoff forecasting
 315 across different coastal seas. Given the unique hydrological characteristics of the
 316 Baltic Sea, largely influenced by its limited connection to the open ocean and signifi-
 317 cant freshwater input from surrounding rivers, the region presents a critical case for
 318 the application of sophisticated forecasting models.

319 The transition from traditional hydrological models to machine learning approaches,
 320 such as the ConvLSTM model, offers significant advantages with respect to the

321 following aspects. The ConvLSTM can be seamlessly integrated into regional cli-
 322 mate models, allowing for the real-time computation of river runoff while performing
 323 climate projections. While the initial training of the model requires substantial
 324 computational resources, it remains less intensive than running comprehensive hydro-
 325 logical models. Furthermore, once trained, the ConvLSTM model is computationally
 326 efficient during inference, ensuring enhanced forecasting capabilities without signifi-
 327 cantly increasing computational demands.

328 However, while the ConvLSTM represents an advancement for the climate com-
 329 munity, given that running and tuning traditional hydrological models demands
 330 extensive expertise, models like E-HYPE maintain an essential role. They provide
 331 a comprehensive dataset that enables to train our ConvLSTM model effectively.
 332 This robust training helps the machine learning models to achieve highly accurate
 333 predictive weights. Thus, rather than rendering traditional methods obsolete, the
 334 integration of machine learning models builds upon and enhances the foundational
 335 data provided by them.

336 6 Conclusions

337 In summary, we showed that the ConvLSTM model demonstrated robust perfor-
 338 mance in forecasting river runoff across 97 rivers entering the Baltic Sea. Trained on
 339 data from 1979 to 2011, the model achieved an impressive daily prediction accuracy
 340 of $\pm 5\%$. Importantly, this accuracy is achieved without any expert's domain knowl-
 341 edge on hydrological modelling. This capability to generate accurate and detailed
 342 simulations enables to examine the potential impacts of different climate scenarios.
 343 Such precision in forecasting and scenario testing is crucial for crafting effective
 344 water resource management strategies and adapting to the changing climate.

345 The robust performance of the ConvLSTM model in simulating river runoff and its
 346 possible effective integration into coupled regional climate models, as for example in
 347 the IOW ESM (Karsten et al., 2024), pave the way for a multitude of new storyline
 348 simulations. Hence, we can now explore various "what-if" scenarios more reliably,
 349 under the assumption that the model weights attained during training are robust.
 350 This represents a significant step forward in our ability to understand and predict
 351 the complex dynamics of river systems and their impact on regional climate systems.

352 7 Acknowledgments

353 The research presented in this study is part of the Baltic Earth program (Earth
 354 System Science for the Baltic Sea region, see <https://www.baltic.earth>.

355 References

- 356 Fang, W., Huang, S., Ren, K., Huang, Q., Huang, G., Cheng, G., & Li, K. (2019).
 357 Examining the applicability of different sampling techniques in the development
 358 of decomposition-based streamflow forecasting models. *Journal of Hydrology*, 568,
 359 534–550. <https://doi.org/10.1016/j.jhydrol.2018.11.020>
- 360 Hagemann, S., Stacke, T., & Ho-Hagemann, H. T. M. (2020). High Resolution Dis-
 361 charge Simulations Over Europe and the Baltic Sea Catchment. *Frontiers in*
 362 *Earth Science*, 8. <https://doi.org/10.3389/feart.2020.00012>
- 363 Karsten, S., Radtke, H., Gröger, M., Ho-Hagemann, H. T. M., Mashayekh, H., Neu-
 364 mann, T., & Meier, H. E. M. (2024). Flux coupling approach on an exchange
 365 grid for the IOW earth system model (version 1.04.00) of the baltic sea region.
 366 *Geoscientific Model Development*, 17(4), 1689–1708. <https://doi.org/10.5194/gmd-17-1689-2024>
- 367 Neumann, T., Koponen, S., Attila, J., Brockmann, C., Kallio, K., Kervinen, M.,
 368 et al. (2021). Optical model for the baltic sea with an explicit CDOM state
 369 variable: A case study with model ERGOM (version 1.2). *Geoscientific Model*
 370 *Development*, 14(8), 5049–5062. <https://doi.org/10.5194/gmd-14-5049-2021>

- 372 SHI, X., Chen, Z., Wang, H., Yeung, D.-Y., Wong, W., & WOO, W. (2015). Con-
373 volutional LSTM Network: A Machine Learning Approach for Precipitation
374 Nowcasting. In *Advances in Neural Information Processing Systems* (Vol. 28).
375 Curran Associates, Inc. Retrieved from <https://proceedings.neurips.cc/paper/2015/hash/07563a3fe3bbe7e3ba84431ad9d055af-Abstract.html>
376
377 Tan, Q.-F., Lei, X.-H., Wang, X., Wang, H., Wen, X., Ji, Y., & Kang, A.-Q. (2018).
378 An adaptive middle and long-term runoff forecast model using EEMD-ANN hy-
379 brid approach. *Journal of Hydrology*, 567, 767–780. <https://doi.org/10.1016/j.jhydrol.2018.01.015>
380